Trans. Korean Soc. Noise Vib. Eng., 25(1) : 13~23, 2015
http://dx.doi.org/10.5050/KSNVE.2015.25.1.013

한국소음진동공학회논문집 제 25 권 제 1 호, pp. 13~23, 2015
ISSN 1598-2785(Print), ISSN 2287-5476(Online)

Measurements of Radial In-plane Vibration Characteristics of Piezoelectric Disk Transducers

원판형 압전 변환기의 면내 방사 진동 특성 측정

Dae Jong Kim*, Se Hwan Oh* and Jin Oh Kim†
김 대 종 · 오 세 환 · 김 진 오

(Received October 7, 2014 ; Revised January 6, 2015 ; Accepted January 6, 2015)

Key Words : Piezoelectricity(압전), Transducer(변환기), Vibration(진동), Resonance(공진), Mode shape(모드 형상), In-plane(면내)

ABSTRACT

The paper experimentally deals with the radial in-plane vibration characteristics of disk-shaped piezoelectric transducers. The radial in-plane motion, which is induced due to Poisson's ratio in the piezoelectric disk polarized in the thickness direction, was measured by using an in-plane laser vibrometer, and the natural frequencies were measured by using an impedance analyzer. The experimental results have been compared with theoretical predictions obtained by simplified theoretical and finite-element analyses. It appears that the fundamental mode of a piezoelectric disk transducer is a radial mode and its radial displacement distribution from the center to the perimeter is not monotonic but shows maximum slightly apart from the perimeter. The theoretically-calculated fundamental frequencies agree well with the finite-element results for small thickness-to-diameter ratio, and they are accurate within 7 % error for the ratio up to 0.4.

요 약

이 논문은 원판형 압전 변환기의 면내 방사 진동 특성을 실험적으로 다룬다. 면내 방사 진동은 두께 방향으로 분극이 된 압전 원판에서 푸아송비로 인해 야기되는 것으로서, 레이저 면내 진동 측정기로써 측정되었고, 고유진동수는 임피던스 분석기로써 측정되었다. 실험 결과는 단순화된 이론적 해석과 유한요소 해석으로부터 얻어진 이론적 예측과 비교되었다. 원판형 압전 변환기의 기본 모드는 방사 모드이고, 중심으로부터 가장자리까지의 반경 방향 변위 분포는 단조 증가가 아니라 원주면에서 약간 떨어진 위치에서 최대 값을 나타낸다. 지름 대비 두께 비율이 작은 원판에서 이론적으로 계산된 기본 진동수는 유한요소 결과와 잘 일치하고, 두께/지름 비율 0.4까지 오차 7 % 이내로 정확하다.

1. Introduction

Piezoelectricity[1] is one of the main transduction mechanisms adopted in electromechanical sensors and actuators[2]. Piezoelectric transducers

† Corresponding Author ; Member, Soongsil University
E-mail : jokim@ssu.ac.kr
Tel : +82-2-820-0662, Fax : +82-2-820-0668
* Member, Soongsil University

‡ Recommended by Editor SungSoo Na

are widely used, especially in ultrasonic sensors[3] which convert mechanical vibrations into electric signals, and actuators[4] which convert electric signal into mechanical vibrations. In many ultrasonic devices, such as flowmeters and liquid-level meters etc., piezoelectric transducers generate and detect mechanical waves[3]. Piezoelectric transducers for ultrasonic devices are designed on the basis of the vibration characteristics of resonance[5].

The vibration characteristics of piezoelectric transducers depend on geometric shapes and dimensions as well as material properties and boundary conditions. Most piezoelectric transducers are disk-shaped[6~9] or ring-shaped[10~12], and their transduction mechanism is based on the motion in the thickness direction. In some cases the shape is cylindrical or spherical. Piezoelectric cylindrical or spherical transducers with radial polarization have resonance characteristics determined by their thickness and curvature[13,14]. Torsional transducers made of piezoelectric disks polarized in the circumferential direction have resonance characteristics determined by thickness[15].

In the piezoelectric disk transducers polarized in the thickness direction, radial motion is induced due to Poisson's ratio[16]. Since the radius is larger than the thickness in a thin disk, the lowest several modes are the radial modes governed mainly by radial boundary conditions. Thickness modes appear in the higher modes. This paper experimentally clarifies the radial in-plane vibration of piezoelectric disk transducers and to verify the theoretical prediction by comparing experimental results with analytical ones.

Theoretical approaches appear in much of the literatures. Reference (6) reported the dependence of the vibrational mode on the disk diameter-to-thickness ratio calculated by the finite-element method. Reference (7) presented vibration characteristics depending on the thickness-graded material properties. Reference (8) showed a generalized form of Hamilton's principle for coupled electromechnical system and compared impedance curves obtained theoretically and experimentally. Reference (9) displayed experimental results obtained by three techniques and compared them with numerical ones. In this literature, mode shapes were shown qualitatively to show vibration distribution. Piezoelectric hollow-disks, so-called ring, were also dealt theoretically in much of literature[10~12].

This paper focuses on the fundamental mode of piezoelectric disk transducers, and presents its radial in-plane vibration motion obtained experimentally by in-plane laser vibrometry. The experimentally-obtained shape of the fundamental mode, which was not available in other literatures, is clearly displayed in this paper. A simplified theoretical analysis[17] is briefly described to compare the experimental results with theoretical predictions. Some of the theoretical and experimental approaches were cited from other literature about ring transducers[18].

2. Theoretical Prediction

In order to compare experimental results with analytical ones, theoretical prediction is carried out in advance. Two kinds of analysis are described in this section; one is theoretical analysis and another is finite-element analysis.

2.1 Theoretical Analysis

(1) Problem formulation

A piezoelectric disk transducer is schematically shown in Fig. 1, where l is the thickness and a is the radius. The transducer has uniform electrodes on the top and bottom surfaces ($z=0,l$). The electromechanical relations were well formulated, and the constitutive equations of the piezoelectric disk transducers are expressed as follows[2]:

$$\mathbf{T} = \mathbf{c}^{E}\mathbf{S} - \mathbf{e}^{T}\mathbf{E} \tag{1}$$

$$\mathbf{D} = \mathbf{e}\,\mathbf{S} + \boldsymbol{\varepsilon}^{S}\mathbf{E} \tag{2}$$

where $\mathbf{T}$, $\mathbf{S}$, $\mathbf{D}$, and $\mathbf{E}$ are the matrices of stresses, strains, electric displacements, and electric fields, respectively. In addition, $\mathbf{c}^{E}$, $\boldsymbol{e}$, and $\boldsymbol{\varepsilon}^{S}$ are the coefficient matrices of the stiffness with constant electric field, the piezoelectric stress constant, and the permittivity with constant strain, respectively.

The axisymmetric vibration in the piezoelectric disk can be formulated in terms of radial displacement $u(r,z,t)$, axial displacement $w(r,z,t)$, and electric potential $\phi(r,z,t)$ with cylindrical coordinates (r,θ,z) and time (t). Normal strains $(\varepsilon_r,\varepsilon_\theta,\varepsilon_z)$, shear strains $(\gamma_{\theta z},\gamma_{zr},\gamma_{r\theta})$, and electric field (E_z) are related as follows:

$$\varepsilon_r = \frac{\partial u}{\partial r},\quad \varepsilon_\theta = \frac{u}{r},\quad \varepsilon_z = \frac{\partial w}{\partial z} \tag{3a,b,c}$$

$$\gamma_{\theta z} = 0,\quad \gamma_{zr} = \frac{\partial u}{\partial z} + \frac{\partial w}{\partial r},\quad \gamma_{r\theta} = 0 \tag{4a,b,c}$$

$$E_z = -\frac{\partial \phi}{\partial z} \tag{5}$$

Inserting Eqs. (1)~(3) into Eqs. (4) and (5) yields normal stresses $(\sigma_r,\sigma_\theta,\sigma_z)$ and electric displacement D_z as follows:

$$\sigma_r = c_{11}^{E}\left(\frac{\partial u}{\partial r}\right) + c_{12}^{E}\left(\frac{u}{r}\right) + c_{13}^{E}\left(\frac{\partial w}{\partial z}\right) + e_{31}\left(\frac{\partial \phi}{\partial z}\right) \tag{6a}$$

$$\sigma_\theta = c_{12}^{E}\left(\frac{\partial u}{\partial r}\right) + c_{11}^{E}\left(\frac{u}{r}\right) + c_{13}^{E}\left(\frac{\partial w}{\partial z}\right) + e_{31}\left(\frac{\partial \phi}{\partial z}\right) \tag{6b}$$

$$\sigma_z = c_{13}^{E}\left(\frac{\partial u}{\partial r}\right) + c_{13}^{E}\left(\frac{u}{r}\right) + c_{33}^{E}\left(\frac{\partial w}{\partial z}\right) + e_{33}\left(\frac{\partial \phi}{\partial z}\right) \tag{6c}$$

$$D_z = e_{31}\left(\frac{\partial u}{\partial r}\right) + e_{31}\left(\frac{u}{r}\right) + e_{33}\left(\frac{\partial w}{\partial z}\right) - \varepsilon_{33}^{S}\left(\frac{\partial \phi}{\partial z}\right) \tag{7}$$

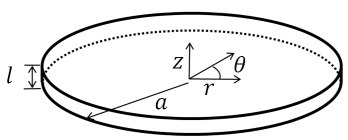

Fig. 1 Schematic diagram of a disk transducer

(2) Solution

The disk transducer, the radius of which is much larger than the thickness, satisfies plane stress conditions in the thickness direction, and thus $\sigma_z = 0$. This assumption simplifies the theoretical analysis. Eq. (6c) can be rewritten to express the normal strain ε_z as follows:

$$\frac{\partial w}{\partial z} = -\frac{c_{13}^{E}}{c_{33}^{E}}\left(\frac{\partial u}{\partial r}\right) - \frac{c_{13}^{E}}{c_{33}^{E}}\left(\frac{u}{r}\right) - \frac{e_{33}}{c_{33}^{E}}\left(\frac{\partial \phi}{\partial z}\right) \tag{8}$$

Eqs. (6a,b) and (7) are rewritten as follows by inserting Eq. (8):

$$\sigma_r = c_{11}^{p}\left(\frac{\partial u}{\partial r}\right) + c_{12}^{p}\left(\frac{u}{r}\right) + e_{31}^{p}\left(\frac{\partial \phi}{\partial z}\right) \tag{9a}$$

$$\sigma_\theta = c_{12}^{p}\left(\frac{\partial u}{\partial r}\right) + c_{11}^{p}\left(\frac{u}{r}\right) + e_{31}^{p}\left(\frac{\partial \phi}{\partial z}\right) \tag{9b}$$

$$D_r = e_{31}^{p}\left(\frac{\partial u}{\partial r}\right) + e_{31}^{p}\left(\frac{u}{r}\right) - \varepsilon_{33}^{p}\left(\frac{\partial \phi}{\partial z}\right) \tag{10}$$

Here the constants with superscript p are as follows:

$$c_{11}^{p} = c_{11}^{E} - \frac{(c_{13}^{E})^2}{c_{33}^{E}} \tag{11a}$$

$$c_{12}^{p} = c_{12}^{E} - \frac{(c_{13}^{E})^2}{c_{33}^{E}} \tag{11b}$$

$$e_{31}^{p} = e_{31} - \frac{c_{13}^{E} e_{33}}{c_{33}^{E}} \tag{11c}$$

$$\varepsilon_{33}^{p} = \varepsilon_{33}^{S} + \frac{e_{33}^2}{c_{33}^{E}} \tag{11d}$$

The equation of motion derived from the force equilibrium in the radial direction is

$$\frac{\partial \sigma_r}{\partial r} + \frac{\sigma_r - \sigma_\theta}{r} = \rho \frac{\partial^2 u}{\partial t^2} \tag{12}$$

where ρ is the mass density. Inserting Eq. (9) into Eq. (12) yields the following governing equation:

$$\frac{\partial^2 u}{\partial r^2} + \frac{1}{r}\frac{\partial u}{\partial r} - \frac{u}{r^2} = \frac{1}{c^2}\frac{\partial^2 u}{\partial t^2} \tag{13}$$

where $c\left(=\left[c_{11}^{p}/\rho\right]^{1/2}\right)$ in the wave Eq. (13) is the propagation speed of the wave.

When the voltage applied to the electrodes is a harmonic function of time t with frequency ω, the displacement w and the electric potential ϕ are regarded as harmonic functions of time with the same frequency. Therefore, $u(r,z,t)$ can be expressed through the separation of variables as seen in the following:

$$u(r,z,t)= U(r)Z(z)e^{j\omega t} \tag{14}$$

Substituting Eq. (14) into Eq. (13) provides the following governing equations in terms of $U(r)$:

$$r^2\frac{d^2U}{dr^2}+r\frac{dU}{dr}+\left(k^2r^2-1\right)U=0 \tag{15}$$

where $k(=\omega/c)$ is the wave number.

The solution of the Bessel Eq. (15) has the following form:

$$U(r)=A\,J_1(kr)+B\,Y_1(kr) \tag{16}$$

where J_1 and Y_1 are the Bessel functions of the first and second kinds, respectively, of order 1. The unknown constants A and B are determined according to the boundary conditions.

(3) Radial mode characteristics

For the transducer free on the circumferential surface $(r=a)$, the boundary conditions are the following:

$$U(0)=0 \qquad \text{at } r=0 \tag{17a}$$

$$\sigma_r(a)=0 \qquad \text{at } r=a \tag{17b}$$

In order to satisfy the boundary condition (17a), $B=0$ in Eq. (16), and thus the solution becomes

$$U(r)=A\,J_1\left(q_n\frac{r}{a}\right) \tag{18}$$

Here $q_n(=ka)$ is the k times the radius a. Satisfying the boundary condition (17b) with Eq. (6a) in the uniform electric field yields

$$\sigma_r(a)=c_{11}^{p}A\,q_n\,J_0(q_n)+\left(c_{12}^{p}-c_{11}^{p}\right)A\,J_1(q_n)=0 \tag{19}$$

The natural frequencies of the radial mode are calculated from Eq. (19). In the characteristic Eq. (19), the unknown variable q_n can be determined by using numerical tools, such as Mathematica[19], and the result is $q_n=2.07, 5.40, 8.58, \ldots$. Frequency f has a relation with wave number k and wave speed c as follows:

$$f=\frac{kc}{2\pi} \tag{20}$$

In addition to the natural frequencies, the radial mode shapes can also be calculated from Eq. (18).

The piezoelectric disk specimens considered in this paper are shown in Fig. 2 and listed in Table 1. The properties of the constituent PZT-4 and PZT-5A materials are well-known, and they are listed in Table 2. The material properties to be inserted into the equations are obtained by converting the properties in Table 2. The converted properties are listed in Table 3.

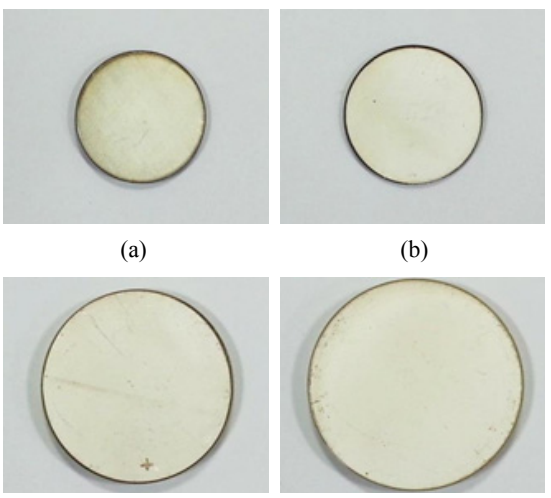

Fig. 2 Specimens of piezoelectric disks; (a) specimen A, (b) specimen B, (c) specimen C, (d) specimen D

The natural frequencies calculated from Eq. (20) are listed in Table 4. The shapes of radial modes calculated from Eq. (18) are displayed in Fig. 3. They will be compared with the experimental results in Section 4.

Table 1 Sizes and material of piezoelectric disk specimens

Specimen	Diameter, $2a$ (mm)	Thickness, t (mm)	Material
A	24.8	2.05	PZT-4
B	27.8	1.4	
C	39.7	4.4	PZT-5A
D	49.7	5.5	

Table 2 Material properties of PZT specimens

Properties			Values	
			PZT-4	PZT-5A
Mechanical	Mas density ($\times 10^3$ kg/m^3)	ρ	7.60	7.70
	Elastic compliance ($\times 10^{-12}$ m^2/N)	s_{11}^E	12.30	16.40
		s_{12}^E	-4.05	-5.74
		s_{13}^E	-5.31	-7.22
		s_{33}^E	15.50	18.80
		s_{44}^E	39.0	47.5
		s_{66}^E	32.9	44.3
Dielectric	Relatice permittivity	k_{33}^E $(=\varepsilon_{33}^S/\varepsilon_0)$	635	830
Electro-mechanical	Piezoelectric strain constant ($\times 10^{-12}$ C/N)	d_{31}	-123.0	-171.0
		d_{33}	289	374
		d_{15}	496	584

Table 3 Material properties of PZT specimens, converted from the properties in Table 2

Properties			Values	
			PZT-4	PZT-5A
Mechanical	Elastic stiffness (10^9 N/m^2)	c_{11}^E	139.0	120.4
		c_{12}^E	77.8	75.2
		c_{13}^E	74.3	75.1
		c_{33}^E	115.4	110.9
		c_{44}^E	25.6	21.1
		c_{66}^E	30.6	22.6
Dielectric	Relatice permittivity ($\times 10^{-9}$C^2/N • m^2)	ε_{33}^S	5.62	7.35
Electro-mechanical	Piezoelectric strain constant (C/m^2)	e_{31}	-5.20	-5.40
		e_{33}	15.10	15.80
		e_{15}	12.70	12.30

Table 4 Natural frequencies of the radial modes calculated for free specimens

Mode	Natural frequency(kHz)			
	A	B	C	D
1	91.3	81.5	49.7	39.8
2	238	217	129	103
3	378	338	205	164

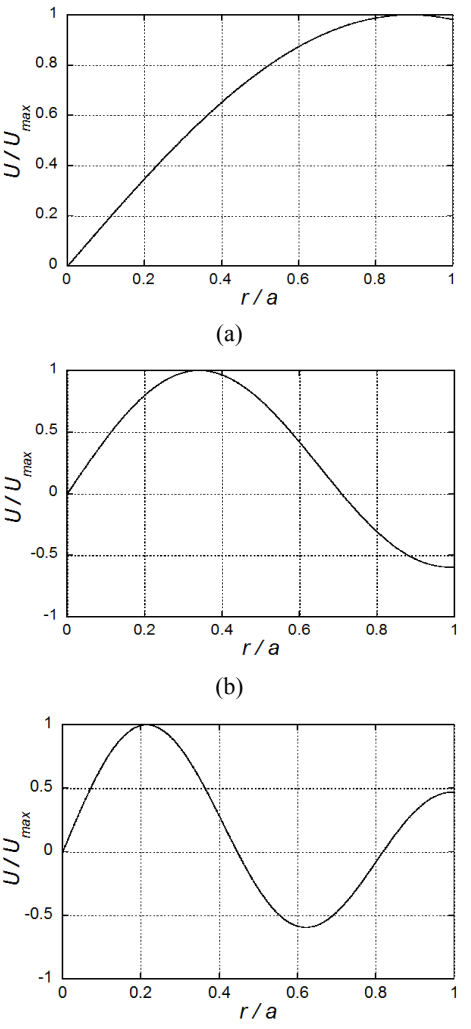

Fig. 3 Radial mode shapes obtained by theoretical analysis ; (a) 1st mode, (b) 2nd mode, (c) 3rd mode

2.2 Finite-element Analysis

The theoretical analysis described in the previous section has advantages in the expressions to calculate the natural frequencies and mode shapes. However, it has disadvantages in that the analysis is based on some assumptions to simplify the real physical phenomenon. Before comparing the theoretically-calculated results with experimental ones, the theoretical analysis is enhanced by a finite-element analysis.

The natural frequencies and mode shapes are obtained by using the commercial software ANSYS. Modal analysis and harmonic analysis were carried out with the boundary conditions that all surfaces are mechanically free and the electric field is established in the thickness direction by the electrodes on the top and bottom surfaces.

Harmonic analysis results are displayed in Fig. 4 in the form of impedance curves for the models of four specimens. In the impedance curves, the minimum points represent the resonances of the transducers. The natural frequencies obtained by the finite-element analysis are listed in Table 5. The fundamental frequencies are 91.0, 81.4, 49.5, and 39.6 kHz for specimens A, B, C, and D, respectively. They are compared with the theoretically-calculated values in Section 4. Incidentally, the mode shapes obtained by the finite-element modal analysis are displayed in Fig. 5. The results of specimen A only are shown in the figure as an example. The shapes of the first three modes in Fig. 5 show radial modes even though other types of modes were not excluded in the analysis.

Table 5 Natural frequencies obtained by the finite element analysis

Mode	Natural frequency(kHz)			
	A	B	C	D
1	91.0	81.4	49.5	39.6
2	236	212	126	101
3	369	336	193	155

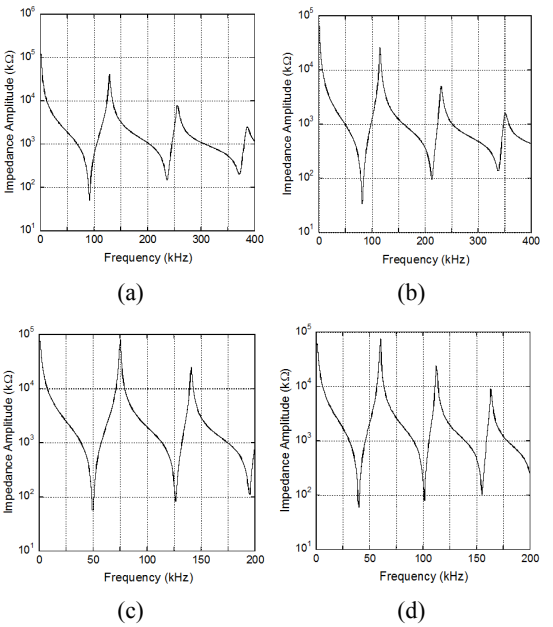

Fig. 4 Impedance curves obtained by the finite element analysis; (a) specimen A, (b) specimen B, (c) specimen C, (d) specimen D

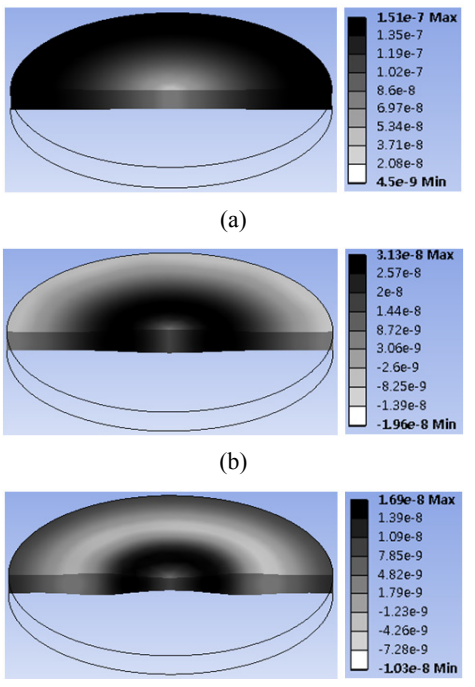

Fig. 5 Mode shapes obtained by the finite-element analysis for specimen A; (a) 1st mode, (b) 2nd mode, (c) 3rd mode

3. Experiments

The vibration characteristics of the piezoelectric disk transducers are experimentally determined in this section, and they are compared with theoretical predictions in the next section. The specimens used in the experiments are shown in Fig. 2, and their sizes and materials are listed in Table 1.

3.1 Impedance Analysis

By using an impedance gain/phase analyzer (Agilent Technology 4192A), impedance curves were measured for four kinds of specimens. The measurements were repeated with three pieces of four specimens. The results of impedance curves obtained with one piece of each specimen are displayed in Fig. 6. In the impedance curves, the minimum points represent the resonances of the transducers. The natural frequencies experimentally -obtained by the impedance curve measurements are listed in Table 6, where the values were averaged from the results of three pieces. The fundamental frequencies are 88.3, 79.6, 48.4, and 38.3 kHz for specimens A, B, C, and D, respectively. They are compared with the theoretically-obtained results in Section 4.

Table 6 Natural frequencies experimentally-obtained by the impedance-curve measurement

Mode	Natural frequency(kHz)			
	A	B	C	D
1	88.3±0.3	79.6±0.2	48.4±0.3	38.3±0.3
2	228.7±0.9	206.6±0.6	122.8±0.4	96.5±0.5
3	355.0±1.3	326.0±0.9	184.8±1.0	146.2±0.6

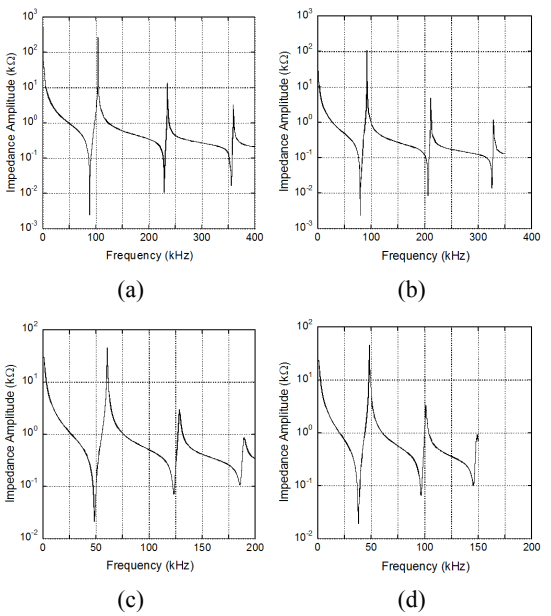

Fig. 6 Impedance curves obtained by experiments; (a) specimen A, (b) specimen B, (c) specimen C, (d) specimen D

3.2 In−plane Laser Interferometry

The mode shapes of the radial in-plane vibration were measured by using an in-plane laser vibrometer. The apparatus used in the experiment is based on the laser interference, and it consists of an optical sensor head (LSV-065-306F) and a controller (OFV-3320) made by Polytec. This apparatus is to measure the moving velocity of the plane perpendicular to the central line bisecting two converging laser beams as shown in Fig. 7. The principle of this apparatus is the Doppler phenomenon, where an optical frequency shift of

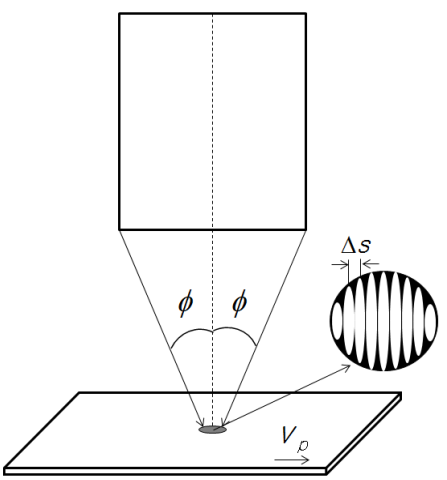

Fig. 7 Schematic diagram of the in-plane laser vibrometer

the back-scattered laser light caused by surface motion is evaluated electronically.

As shown in Fig. 7, the laser output from a diode is divided into two beams. These two beams progress with incident angle ϕ into the plane to be measured, and the superposition of the beams results in the interference pattern of parallel bright and dark fringes. The fringe spacing $\triangle s$ is a system constant which depends only on the incident angle ϕ and laser wavelength λ as follows:

$$\triangle s = \frac{\lambda}{2 \bullet \sin\theta} \tag{21}$$

When the plane moves with velocity v_p in the in the direction normal to the interference fringe, the change of the light scattering on the periodic fringe makes the photo detector of the sensor head generate signals of Doppler frequency f_D proportional to the velocity v_p. The moving velocity and the Doppler frequency have the following relation:

$$v_p = f_D \bullet \triangle s \tag{22}$$

The controller measures the Doppler frequency f_D and multiplies $\triangle s$. The output signal of the controller is monitored at an oscilloscope or a signal analyzer.

A signal generator (Agilent 33220A) was used to exert electric signals with a constant voltage and variable frequency onto piezoelectric disks. The output signal of the controller was monitored on an oscilloscope (Tektronix TDS3032) and the frequency of the signal resulting at the maximum amplitude was determined as the natural frequency of the disk. The fundamental frequencies of the disks measured in this way are 88.2, 79.4, 47.9, and 38.0 kHz for specimen A, B, C, and D, respectively. These results are listed in Table 7 and will be compared with other results in Section 4.

Vibration amplitude at the natural frequency was measured by using a signal analyzer (B&K 2035). The measured amplitude is RMS voltage, which is proportional to the vibration velocity, and is converted to the vibration displacement. The measurement is carried out along a radius from the center to the perimeter at every 1 mm. The measured vibration amplitude was normalized to the maximum amplitude and displayed in Fig. 8

Table 7 Comparison of the fundamental frequencies obtained by calculation, finite-element method, and measurement for three specimens with free boundary conditions

Specimen	Fundamental frequency(kHz)			
	Calculation	FEM	Measurement	
			Impedance curve	In-plane vibrometer
A	91.3	91.0	88.3±0.3	88.2±0.4
B	81.5	81.4	79.6±0.2	79.4±0.3
C	49.7	49.5	48.4±0.3	47.9±0.2
D	39.8	39.6	38.3±0.3	38.0±0.4

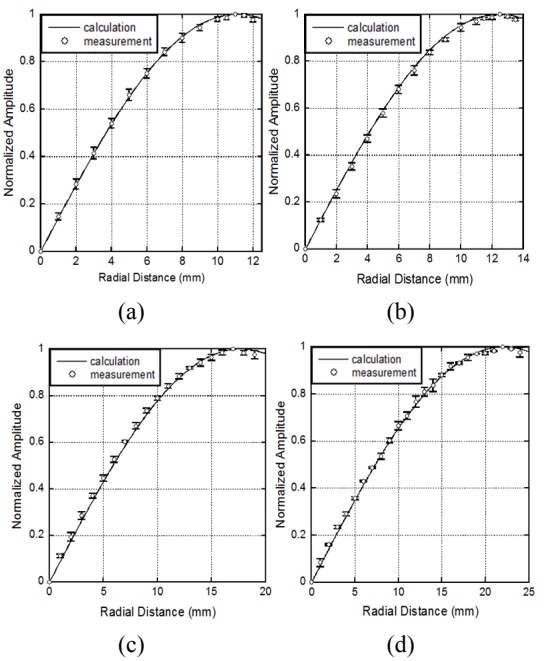

Fig. 8 Radial mode shapes of the fundamental mode measured by the laser vibrometer; (a) specimen A, (b) specimen B, (c) speimen C, (d) specimen D

for four specimens. In Fig. 8, the solid line is the theoretically-calculated result obtained in Section 2.1. The mode shapes displayed in Fig. 8 are discussed in Section 4.

4. Comparisons and Discussions

Natural frequencies and mode shapes obtained theoretically in Section 2 and experimentally in Section 3 are compared with each other and discussed in this section.

The fundamental frequencies obtained by calculation, the finite-element method, and measurement

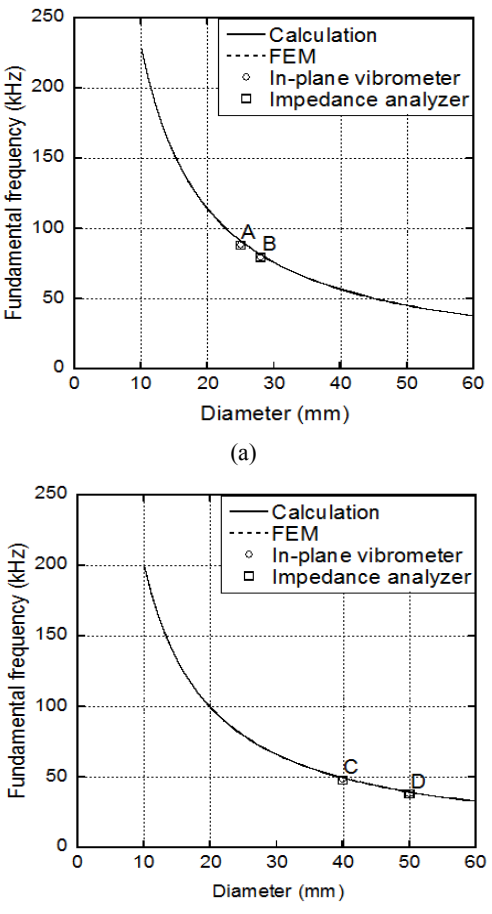

Fig. 9 Comparison of the fundamental frequencies obtained by calculation, finite-element method, and measurements; (a) PZT-4, (b) PZT-5A

for four specimens are listed in Table 7 and displayed in Fig. 9. The experimental results agree well with the theoretical predictions. The fundamental frequency of the piezoelectric disk transducer depends on its radius, and the frequency is higher as the radius is smaller. The theoretically-calculated fundamental frequencies are compared with the finite-element results in Fig. 9. The theoretically-calculated results agree well with the finite-element results for small thickness-to-diameter ratio, and they are accurate within 7 % error for the ratio up to 0.4.

The mode shapes obtained by the laser vibrometer are compared with the theoretical predictions in Fig. 8. The results agree well with each other. The displacement distribution from the center to the perimeter is not monotonic. The vibration amplitude is maximum slightly apart from the perimeter.

5. Conclusion

The paper presented the radial in-plane vibration characteristics of disk-shaped piezoelectric transducers polarized in the thickness direction. The radial in-plane vibration characteristics of piezoelectric disk transducers were experimentally investigated by measuring natural frequencies and mode shapes. The natural frequencies of piezoelectric transducers were measured by using an impedance analyzer and compared with theoretical predictions. The radial in-plane motion, which was induced due to Poisson's ratio in the piezoelectric disk polarized in the thickness direction, was measured by using an in-plane laser vibrometer and compared with theoretically obtained results.

The fundamental mode shape of a piezoelectric disk is a radial mode and the radial displacement distribution from the center to the perimeter is not monotonic but shows maximum slightly apart from the perimeter. The fundamental frequencies

obtained by the simplified theoretical analysis briefly described in this paper well agreed in small thickness-to-diameter ratio range with other results obtained by finite-element analysis and experiments. In the range of the ratio over 0.4, the theoretically-obtained natural frequencies showed errors more than 7 %. The theoretical analysis may be used to predict the vibration characteristics of thin piezoelectric disk transducers.

Acknowledgment

This research was supported by the MSIP (Ministry of Science, ICT & Future Planning), Korea, under the Convergence-ITRC (Convergence Information Technology Research Center) support program (NIPA-2014-H0401-14-1005) supervised by the NIPA (National IT Industry Promotion Agency).

References

(1) Ikeda, T., 1996, Fundamentals of Piezoelectricity, Oxford University Press, Oxford.

(2) Busch-Vishniac, I. J., 1999, Electromechanical Sensors and actuators, Springer, New York, Chapter 5.

(3) Lynnworth, L. C., 1989, Ultrasonic Measurements for Process Control, Academic Press, Boston.

(4) Choi, S.-B. and Han, Y.-M., 2010, Piezoelectric Actuators : Control Applications of Smart Materials, Boca Raton: Taylor & Francis.

(5) Miu, D. K., 1993, Mechatronics: Electromechanics and Contromechanics, Springer, New York, Chapter 6.

(6) Kunkel, H. A., Locke, S. and Pikeroen, B., 1999, Finite-element Analysis of Vibrational Modes in Piezoelectric Ceramic Disks, IEEE Transactions on Ultrasonics, Ferroelectrics, and Frequency Control, Vol. 37, pp. 316~328.

(7) Lee, P. C. Y., Yu, J.-D., Li, X. and Shih, W.-H., 1999, Piezoelectric Ceramic Disks with Thickness-graded Material Properties, IEEE Transactions on Ultrasonics, Ferroelectrics, and Frequency Control, Vol. 46, pp. 205~215.

(8) Ho, S.-T., 2007, Modeling of a Disk-type Piezoelectric Transformer, IEEE Transactions on Ultrasonics, Ferroelectrics, and Frequency Control, Vol. 54, pp. 2110~2119.

(9) Lin, Y.-C. and Ma, C.-C., 2004, Experimental Measurement and Numerical Analysis on Resonant Characteristics of Piezoelectric Disks with Partial Electrode Designs, IEEE Transactions on Ultrasonics, Ferroelectrics, and Frequency Control, Vol. 51, pp. 937~947.

(10) Iula, A., Lamberti, N. and Pappalardo, M., 1996, A Model for the Theoretical Characterization of Thin Piezoceramic Rings, IEEE Transactions on Ultrasonics, Ferroelectrics, and Frequency Control, Vol. 43, pp. 370~375.

(11) Li, H. L., Hu, J. H. and Chan, H. L. W., 2004, Finite Element Analysis on Piezoelectric Ring Transformer, IEEE Transactions on Ultrasonics, Ferroelectrics, and Frequency Control, Vol. 51, pp. 1247~1254.

(12) Ho, S.-T., 2007, Modeling and Analysis on Ring-type Piezoelectric Transformers, IEEE Transactions on Ultrasonics, Ferroelectrics, and Frequency Control, Vol. 54, pp. 2376~2384.

(13) Kim, J. O. and Lee, J. G., 2007, Dynamic Characteristics of Piezoelectric Cylindrical Transducers with Radial Polarization, Journal of Sound and Vibration, Vol. 300, pp. 241~249.

(14) Kim, J. O., Lee, J. G. and Chun, H. Y., 2005, Radial Vibration Characteristics of Spherical Piezoelectric Transducers, Ultrasonics, Vol. 43, pp. 531~537.

(15) Kim, J. O. and Kwon, O. S., 2003, Vibration Characteristics of Piezoelectric Torsional Transducers, Journal of Sound and Vibration, Vol. 264, pp. 453~473.

(16) Meitzler, A. H., O'Bryan, Jr., H. M. and Tiersten, H. F., 1973, Definition and Measurement of Radial Mode Coupling Factors in Piezoelectric Ceramic Materials with Large Variations in Poisson's Ratio, IEEE Transactions on Sonics and Ultrasonics, Vol. SU-20, pp. 233~239.

(17) Kim, J. O., Oh, S. H. and Piao, C., 2013, Radial Mode Vibration Characteristics of Disc-type

Piezoelectric Transducers, Proceedings of the 15th Asia Pacific Vibration Conferences, pp. 1058~1061.

(18) Piao, C. and Kim, J. O., 2014, In-plane Vibration Characteristics of Piezoelectric Ring Transducers, Transactions of the Korean Society for Noise and Vibration Engineering, Vol. 24, No. 10, pp. 780~787.

(19) Wolfram, S., 1999, The Mathematica Book, 4th ed., Wolfram Media Inc., Champaign.

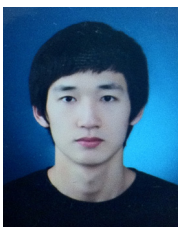

Dae Jong Kim received the B.S. degree in mechanical engineering from Soongil University in 2013. During his stay at Soongsil as a graduate student, he has been working on the vibration characteristics of piezoelectric transducers.

Se Hwan Oh received the B.S. and M.S. degrees in mechanical engineering from Soongil University in 2011 and 2013, respectively. During his stay at Soongsil as a graduate student, he has been working on the vibration characteristics of piezoelectric transducers. Since 2013 he has been working in Hyundai Wia Co. Ltd.

Jin Oh Kim received the B.S. and M.S. degrees in mechanical engineering from Seoul National University in 1981 and 1983, respectively, and the Ph.D. degree from University of Pennsylvania in 1989. Since 1997, he has been with the Faculty of Soongsil University, where he is currently a Professor of mechanical engineering. His research interests are in the areas of ultrasonic sensors and actuators using mechanical vibrations and human-body dynamics for rehabilitation robots.